ACS APPLIED MATERIALS & INTERFACES

Research Article

www.acsami.org

Gas Sensors Based on Metal Sulfide $Zn_{1-x}Cd_xS$ Nanowires with Excellent Performance

Linghui Zhu,[†,‡] Ying Wang,[‡] Dezhong Zhang,[†] Chao Li,[‡] Dongming Sun,[†] Shanpeng Wen,[*,†] Yu Chen,[*,§] and Shengping Ruan[*,‡]

[†]State Key Laboratory on Integrated Optoelectronics, and [‡]College of Electronic Science and Engineering, Jilin University, Changchun 130012, P. R. China

[§]Institute of Semiconductors, Chinese Academy of Sciences, Beijing 100083, P. R. China

Supporting Information

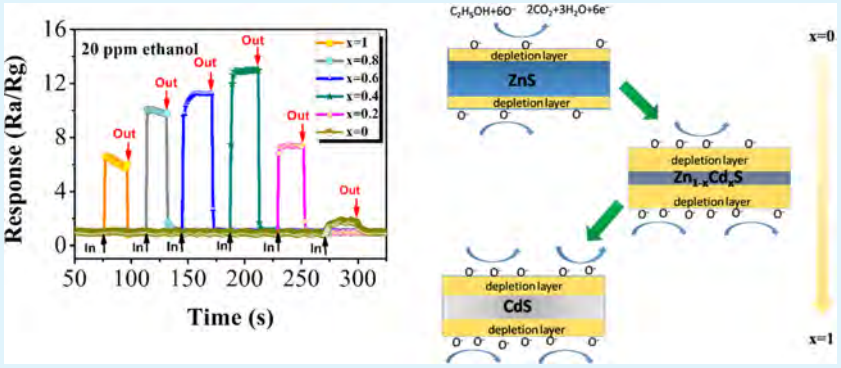

ABSTRACT: Metal sulfide $Zn_{1-x}Cd_xS$ nanowires (NWs) covering the entire compositional range prepared by one step solvothermal method were used to fabricate gas sensors. This is the first time for ternary metal sulfide nanostructures to be used in the field of gas sensing. Surprisingly, the sensors based on $Zn_{1-x}Cd_xS$ nanowires were found to exhibit enhanced response to ethanol compared to those of binary CdS and ZnS NWs. Especially for the sensor based on the $Zn_{1-x}Cd_xS$ (x = 0.4) NWs, a large sensor response (s = 12.8) and a quick rise time (2 s) and recovery time (1 s) were observed at 206 °C toward 20 ppm ethanol, showing preferred selectivity. A dynamic equilibrium mechanism of oxygen molecules absorption process and carrier intensity change in the NWs was used to explain the higher response of $Zn_{1-x}Cd_xS$. The reason for the much quicker response and recovery speed of the $Zn_{1-x}Cd_xS$ NWs than those of the binary ZnS NWs was also discussed. These results demonstrated that the growth of metal sulfide $Zn_{1-x}Cd_xS$ nanostructures can be utilized to develop gas sensors with high performance.

KEYWORDS: *solvothermal, metal sulfide, $Zn_{1-x}Cd_xS$, gas sensing, high response, quick rise and recovery time*

INTRODUCTION

Because of the unique electrical, chemical and optical properties, the one-dimensional (1D) II−VI metal sulfide semiconductor nanostructures have attracted considerable attentions for efficient use in kinds of nanodevices.[1] Among various metal sulfides, zinc sulfide (ZnS) has shown remarkable fundamental property versatility, such as wide direct band gap, the presence of polar surfaces, excellent transport properties, good thermal stability, and so forth.[2,3] Therefore, 1D ZnS has been of growing interest owing to prominent applications in solar cells,[4] field emitters,[5] field-effect transistors,[6] biodevices,[7] light detectors,[8] and so on. However, there are relatively few reports about the gas sensing properties of metal sulfide including ZnS. In the past years, the studies of gas sensing materials focused primarily on traditional metal oxides such as ZnO,[9] SnO_2,[10] TiO_2,[11] and In_2O_3.[12] Nanoscale ZnO is one of the most popular sensing materials used in gas detecting field due to the structure richness and novel properties.[13−16] ZnS is known to have close fundamental physical properties with ZnO, including crystal structures, lattice constants, and so forth. Thus, the prospective morphologies and novel properties of ZnS nanostructure may rival those of ZnO. Therefore, ZnS may be a good candidate for gas sensing. However, the few reported ZnS NWs sensors always suffer from the disadvantages of the low response, slow rise or recovery speed.[17] These disadvantages would limit the practical application of ZnS in detecting gas. Therefore, it is necessary to find some ways to improve the sensing properties of the ZnS nanostructures.

It is known that the gas response of a semiconductor sensing film is manifested by the change in electric conductance which is affected by the interaction between the adsorbed target gas molecules and active sites on the sensing film surface. What's more, a semiconducting alloy with variable elementary composition provides an extra way to tune the physical, electrical,

Received: June 30, 2015
Accepted: September 2, 2015
Published: September 2, 2015

DOI: 10.1021/acsami.5b05845
ACS Appl. Mater. Interfaces 2015, 7, 20793−20800

and chemical properties. Hence, it is well-understood that gas sensing properties can be tuned significantly by the chemical components of the sensing film. For example, Simon et al. have prepared a series of nanoparticulate $LnMO_3$ (Ln = La, Pr, Nd, Sm, Eu, Gd, Tb, Dy, Ho, Er, Tm, Yb, Lu; M = Fe, Cr) oxides and demonstrated a controllable sensing behaviors via chemical tuning.[18] A $CdIn_2O_4$ nanocrystal sensor was reported to show better ethanol sensing performance than the competing SnO_2 and In_2O_3 sensors.[19] $In_{2-x}Ni_xO_3$ nanofibers were proved to show much higher response to NO_2 than In_2O_3 nanofibers.[12]

To improve the sensing performances, $Zn_{1-x}Cd_xS$ NW is considered to be a viable alternative for the conductometric sensors. Cd is known to be a more electronegative element than Zn and the CdS NWs have shown very fast response speed to ethanol despite of the relative low response.[20] Compositional combinations between Zn-sulfide and Cd-sulfide with different chemical and electrical properties are expected to provide a unique strategy to design high performance gas sensors.[21] Therefore, $Zn_{1-x}Cd_xS$ with varied stoichiometric ratio of the system may realize the favorable sensing characteristics. In this work, a series of $Zn_{1-x}Cd_xS$ nanowires (NWs) covering the entire compositional range were prepared by one step solvothermal method and they were used to fabricate gas sensors for the first time. The novel sensors based on $Zn_{1-x}Cd_xS$ nanowires (especially when x = 0.4) exhibited enhanced response to ethanol compared to binary ZnS NWs. The corresponding mechanism for the enhanced sensing properties was discussed. The effects of relative humidity and repeatability on the sensor performance were also investigated.

EXPERIMENTAL SECTION

All the chemicals were of analytical grade and used without any further purification. First, six flasks were used and appropriate amounts of thiourea (tu, NH_2CSNH_2), zinc acetate [$(CH_3COO)_2Zn{\cdot}2H_2O$], and cadmium acetate [$(CH_3COO)_2Cd{\cdot}4H_2O$] were placed in each flask. The proportions of zinc cation among the total metal cationic sources (zinc and cadmium cation) were different (100%, 80%, 60%, 40%, 20%, and 0%) in every flask. Second, a 32 mL mixture of ethylenediamine (en, $NH_2CH_2CH_2NH_2$) and water with a volume ratio of 2:1 was added into each of the above flasks. After been stirred for 20 min, the obtained mixture was transferred to a Teflon vessel with a 40 mL capacity. Every vessel was sealed in a stainless steel autoclave and heated at 175 °C for 8 h, and then cooled to room temperature. The products were washed several times with ethanol and water and dried at 60 °C in air.

The products were analyzed using a powder X-ray diffractometer (XRD, Shimadzu XRD-6000) with Cu Kα radiation. The morphology and the structure of the products were analyzed by using a field-emission scanning electron microscope (SEM, XL 30 ESEM FEG), and energy dispersive spectra (EDS) analysis had also been done in the this equipment. A transmission electron microscope (TEM, JEM-2100) was used to observe the morphologies of the sample and conduct the energy dispersive X-ray (EDX) analysis.

To produce the gas sensors, every as-synthesized sample was mixed with deionized water in a weight ratio of 2:1 after sonication to form a paste. The paste was coated onto a ceramic tube with a pair of Au electrodes attached for resistance measurements. Then a Ni−Cr heating wire was inserted in the tube as a heater. After being welded on the pedestal, the gas sensors were aged for 100 h at the work temperature of 120 °C. The schematic structure of the NWs gas sensor is shown in Figure S1.

A static test system CGS-8 (Chemical gas sensor-8, Beijing Elite Tech Co., Ltd., China) was used to measure the gas sensing properties of the different devices. For the sensor, the response of the sensor is defined as $R = R_a/R_g$, where R_a and R_g are the electrical resistances of the sensor in air and in the presence of a detected gas, respectively. Before the test, glass bottles (1 L) with different concentrations of target gas were prepared. The corresponding process is presented in the Supporting Information. During the test, the sensor was put into the above test bottle. When the sensitivity reached a constant value, the sensor was taken out to recover in air. The time taken by the sensor to achieve 90% of the total response change was defined as the response time τ_{res} in the case of response or the recovery time τ_{rec} in the case of recovery.

RESULTS AND DISCUSSION

A series of $Zn_{1-x}Cd_xS$ samples (where x = 0, 0.2, 0.4, 0.6, 0.8, and 1.0 in the precursor solutions) were obtained via the solvothermal method. The as-prepared samples dispersing in water are shown in Figure 1a. It can be seen that the colors of the samples are different, changing from white to yellow when x increase from 0 to 1. The structures of these products can be verified by the morphological analyses presented by the SEM images shown in Figure 1b−f, respectively. These nanowires are 20−80 nm in diameter and hundreds of nanometers in length. The corresponding EDX data are shown in the Supporting Information, Figure S2 and Table S1.

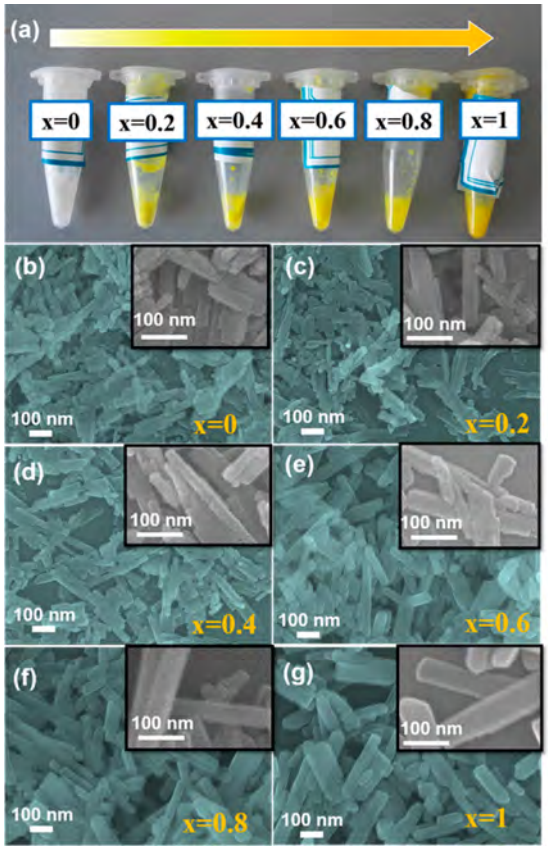

Figure 1. (a) Products dispersed in water with different x values. SEM images of $Zn_{1-x}Cd_xS$ NWs (b) x = 0, (c) x = 0.2, (d) x = 0.4, (e) x = 0.6, (f) x = 0.8, and (g) x = 1. Corresponding detailed SEM images are shown in the insets.

The crystalline phase and crystallographic orientation of the $Zn_{1-x}Cd_xS$ NWs were investigated by XRD analysis, displayed in Figure 2a. When only zinc acetate was used as the cationic source, it is clearly seen that the diffraction peaks of the $Zn_{1-x}Cd_xS$ (x = 0) are consistent with a hexagonal wurtzite phase of ZnS in the JCPDS card (no. 36-1450), with lattice constants of a = 3.821 Å and c = 6.257 Å (shown in Figure 2b). No other crystalline impurities are detected. This indicates that the ZnS NWs crystallize in the pure hexagonal wurtzite form, belonging to the

DOI: 10.1021/acsami.5b05845
ACS Appl. Mater. Interfaces 2015, 7, 20793−20800

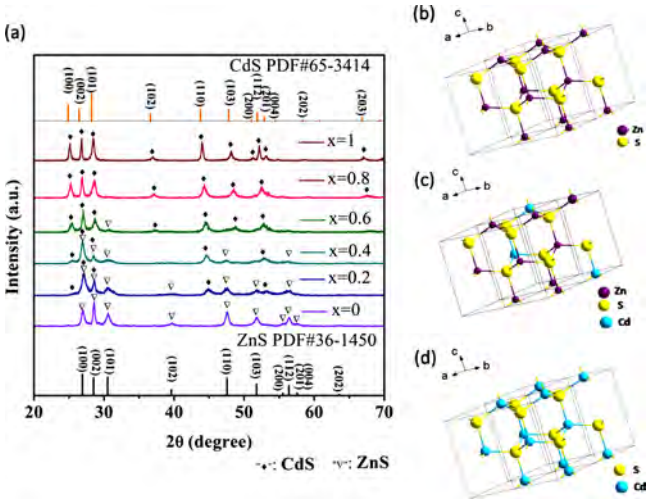

Figure 2. (a) XRD patterns of $Zn_{1-x}Cd_xS$ NWs (x = 0−1). Configurations of hexagonal wurtzite (b) ZnS, (c) $Zn_{1-x}Cd_xS$, and (d) CdS.

space group *P*63*mc* (186). When x = 1, the XRD peaks of the sample with Cd^{2+} alone as the cationic source can be indexed to crystalline hexagonal wurtzite structure of CdS in the JCPDS card (no. 65-3414), with lattice constants of a = 4.132 Å and c = 6.734 Å (shown in Figure 2d). No other crystalline impurities are detected. Interestingly, when zinc acetate and cadmium acetate are used as the cationic source at the same time, it is to be noted that XRD peaks corresponded to wurtzite ZnS shift toward smaller diffraction angles and the diffraction intensities become relatively weaker with the increase of x value from 0.2 to 0.8. Meanwhile, diffraction peaks indexed to wurtzite CdS become relatively stronger and also showing shift to smaller diffraction angles. This phenomenon indicated the formation of $Zn_{1-x}Cd_xS$ phases (shown in Figure 2c) with the incorporation of Cd sources along with the zinc sources.[22] Because of the incorporation of Cd^{2+} ions (0.92 Å at tetrahedral sites) with larger ionic radii than Zn^{2+} ions (0.74 Å at tetrahedral sites) in the ZnS lattice, the lattice constant increased and hence the peak shift toward a smaller diffraction angle.[23] What's more, there are shifted diffraction peaks indexed to wurtzite ZnS and CdS detected at the same time when x = 0.2, 0.4, and 0.6, indicating the formation of composite metal sulfide.

As the semiconductor sensors always work at a high temperature in air, studying the thermal stability of the $Zn_{1-x}Cd_xS$ (x = 0−1) NWs becomes necessary for their gas sensing application. In our experiment, the $Zn_{1-x}Cd_xS$ powder products were heated at 300, 380, and 460 °C in air for 2 h. The corresponding XRD patterns are shown in Figure 3, illustrating that the $Zn_{1-x}Cd_xS$ NWs had no crystal phase transition at a high temperature below 380 °C. However, when the calcination temperature increased to 460 °C, diffraction peaks indexed to other phases appeared, indicating the instability of the $Zn_{1-x}Cd_xS$ NWs at such a high temperature. Therefore, the work temperature of the $Zn_{1-x}Cd_xS$ (x = 0−1) NWs based gas sensors should be less than 380 °C to keep the stability of the sensing film in air.

The structure and morphology of the NWs were further characterized by TEM. Figure 4a−c displays the high-resolution TEM (HRTEM) images recorded from individual $Zn_{1-x}Cd_xS$ NW with x = 0, 0.4, and 1 in order to study the crystal structures of NWs. The corresponding insets show the TEM images of uniform NWs. Figure 4a shows the HRTEM image of a ZnS NW exhibiting its wurtzite crystal structure. Measured lattice spacing was 0.63 nm for the lattice planes perpendicular to the axis of the NW, representing the (001) lattice plane of wurtzite ZnS.[24] Figure 4b shows the HRTEM image of a $Zn_{1-x}Cd_xS$ NW with x = 0.4, confirming the wurtzite structure of the NW and the growth direction of [001]. Likewise, the measured interplanar distance (0.66 nm) for the NW lattice in Figure 4c corresponds to the (001) lattice spacing of the hexagonal CdS crystal, which has a direction parallel to the long axis of the NWs.[25] The HRTEM images clearly indicates the hexagonal structure of the NWs. Figure 4d shows the HRTEM image of a single $Zn_{1-x}Cd_xS$ (x = 0.4) NW and the growth direction of [001]. The corresponding elemental maps displayed in Figure 4e−g further clearly demonstrate the spatial distribution of all constituting elements of $Zn_{1-x}Cd_xS$ (x = 0.4) NW. The S K-edge, Zn K-edge, and Cd L-edge signals are seen uniformly distributed along the whole NW, indicating the three elements are homogeneously distributed in the NW.

As the operating temperature of semiconductor sensors has a large impact on the reaction between the absorbed gas and sensing materials, the gas-sensing properties are greatly influenced by the operating temperature. In our work, the relationship between response and operating temperature of sensors under a relative humidity of 25% RH are shown in Figure 5a. It can be found that the responses of the gas sensors varied with operating temperature. First, the responses gradually increased with temperature. After that, max responses were obtained at 206 °C. When the working temperature increased further, the responses decreased gradually. Therefore, 206 °C is determined to be the optimum operating temperature. Figure 5b shows the responses of the sensors as a function of ethanol gas concentration at 206 °C. The responses increase quickly with the concentration increasing in the range of 2−200 ppm. When the concentrations became larger, the speed of response growth

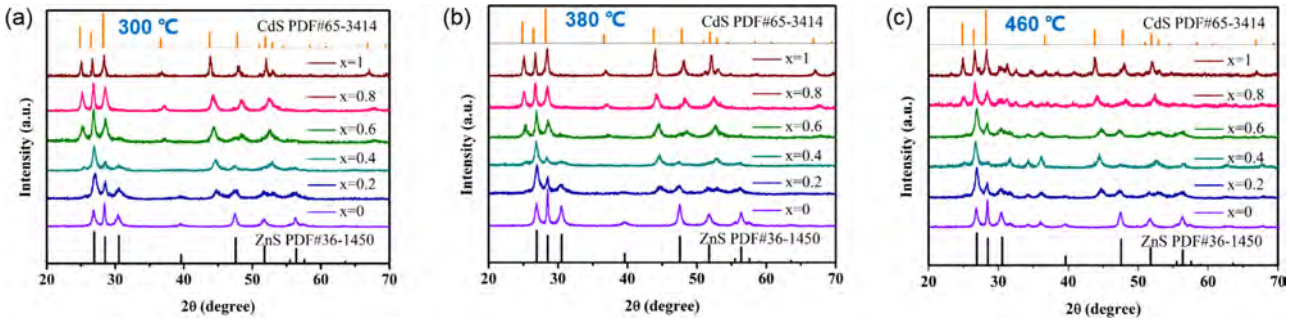

Figure 3. XRD patterns of $Zn_{1-x}Cd_xS$ NWs (x = 0−1) calcined at (a) 300 °C, (b) 380 °C, and (c) 460 °C for 2 h.

DOI: 10.1021/acsami.5b05845
ACS Appl. Mater. Interfaces 2015, 7, 20793−20800

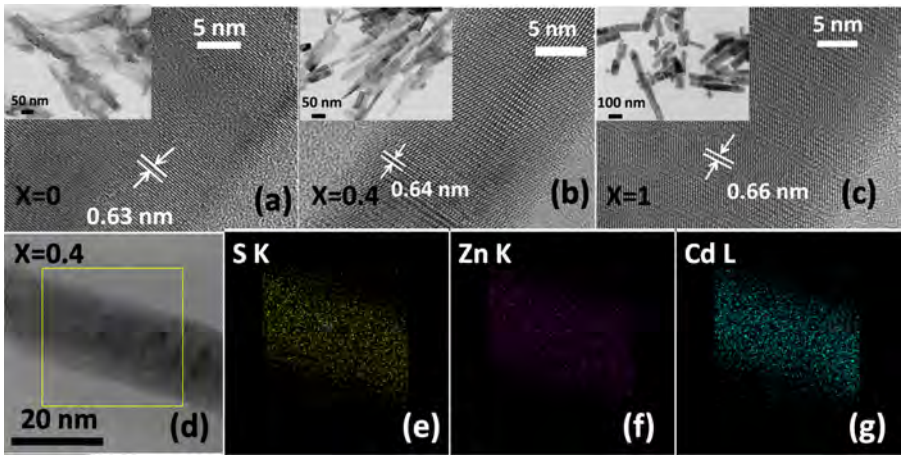

Figure 4. HRTEM images of wurtzite (a) $x = 0$, (b) $x = 0.4$, and (c) $x = 1$ $Zn_{1-x}Cd_xS$ NWs. The insets are the corresponding TEM images showing uniform NWs. (d) TEM image of an individual $Zn_{1-x}Cd_xS$ ($x = 0.4$) NW. (e−g) Elemental maps of the same NW region, indicating spatially resolved elemental distribution of S (yellow), Zn (purple), and Cd (cyan).

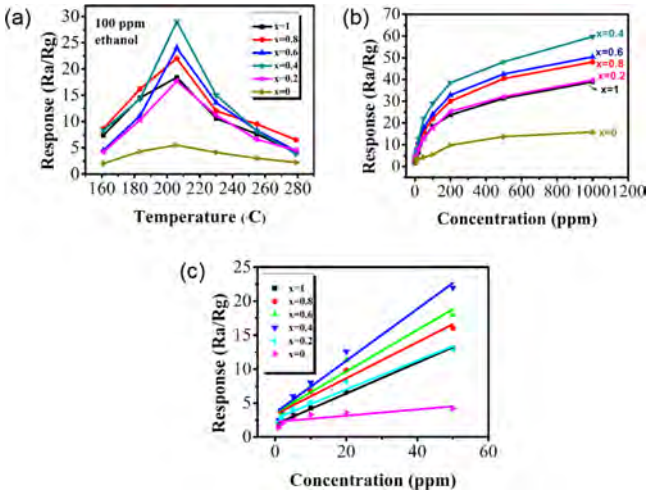

Figure 5. Performance of gas sensors under a relative humidity of 25% RH: (a) Response of the NW based sensors to 100 ppm ethanol gas in air as a function of operating temperature. (b) Response of the gas sensors vs ethanol concentration from 2 to 1000 ppm at an operating temperature of 206 °C. (c) Linear dependence of the response on the ethanol concentration in the range 2−50 ppm.

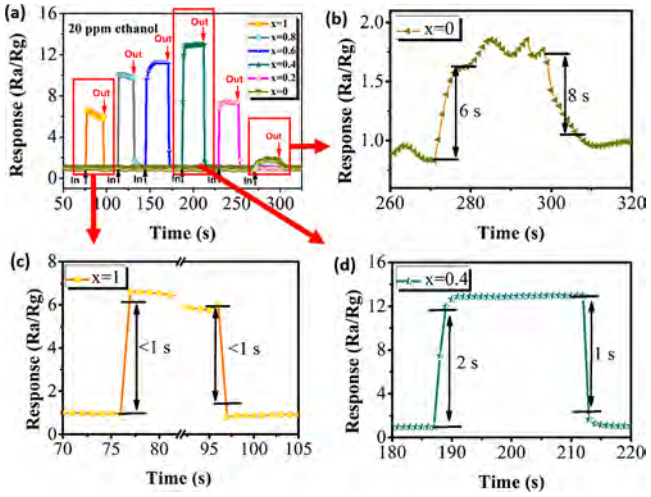

Figure 6. (a) Response transient curves of the six sensors to 20 ppm ethanol at the operating temperature of 206 °C under a relative humidity of 25% RH. Single transient curves of sensors based on $Zn_{1-x}Cd_xS$ with (b) $x = 0$, (c) $x = 1$, and (d) $x = 0.4$.

slowed down. It can be found in Figure 5c that the responses increased linearly with the ethanol concentration from 2 to 50 ppm, which makes such devices very practical.

Response and recovery speeds are important parameters to evaluate the performance of gas sensors. Under a relative humidity of 25% RH, different single response transient curves of the six sensors based on $Zn_{1-x}Cd_xS$ NWs to 20 ppm ethanol at the operating temperature of 206 °C are shown in Figure 6a. The response values of the sensors underwent drastic increase when exposed to ethanol and then dropped to their initial values after the sensor was exposed back to air. The corresponding detailed values are summarized in Table 1. It can be found that the responses of ZnS are changed greatly by Cd incorporation. The response to 20 ppm ethanol of $Zn_{1-x}Cd_xS$ with $x = 0.2$, 0.4, 0.6, 0.8, and 1 is about 7.5, 12.8, 11.3, 9.8, and 6.6, respectively, much larger than the value of 2.1 for ZnS. The highest response to ethanol, greater than those of pure ZnS and CdS, was achieved by the NWs with $x = 0.4$. The single response transient curves of sensors based on $Zn_{1-x}Cd_xS$ NWs with $x = 0$, $x = 1$, and $x = 0.4$ are shown in Figure 6b−d, respectively. From the perspective of practical application of sensor devices, not only high response but also fast response and recovery speed are vital in avoiding possible loss and disasters. The $Zn_{1-x}Cd_xS$ ($x > 0$) sensors exhibit very quick response behavior to ethanol gas. The response and recovery time of $Zn_{1-x}Cd_xS$ ($x = 0.4$) is calculated to be 2 and 1 s, respectively. Compared with the various reported sensors (shown in Table 2), the sensor based on $Zn_{1-x}Cd_xS$ ($x = 0.4$) NWs has the advantages of having fast rise and recovery speed at the same time.

From the results above, we can see that the devices based on $Zn_{1-x}Cd_xS$ NWs with high responses, quick response, and

Table 1. Sensing Properties of the $Zn_{1-x}Cd_xS$ ($x = 0−1$) NWs Sensors to 20 ppm Ethanol at 206 °C

	material					
	$x = 0$	$x = 0.2$	$x = 0.4$	$x = 0.6$	$x = 0.8$	$x = 1$
response (R_a/R_g)	2.1	7.5	12.8	11.3	9.8	6.6
rise time	6 s	1 s	2 s	2 s	<1 s	<1 s
recovery time	8 s	1 s	1 s	1 s	1 s	<1 s

DOI: 10.1021/acsami.5b05845
ACS Appl. Mater. Interfaces 2015, 7, 20793−20800

Table 2. Comparison of the Reported Ethanol Gas Sensors

material	work temperature	ethanol concn	response (R_a/R_g)	rise time	recovery time	ref
$ZnSnO_3$ nanorods	250 °C	500 ppm	109	5 s	15 s	29
$CdIn_2O_4$ nanoparticle	260 °C	1000 ppm	150	6 s	30 s	19
flower-like SnO_2 nanostructure	240 °C	100 ppm	42.6	2 s	15 s	30
Au/ZnO nanostructures	300 °C	50 ppm	8.9	10 s		31
CdOfilm	400 °C	1000 ppm	1.28	19 s	103 s	32
$CoFe_2O_4$ nanopowders	150 °C	50 ppm	71.9	50 s	60 s	33
Co_3O_4	280 °C	100 ppm		121 s	203 s	34
Co_3O_4@carbon foam	320 °C	100 ppm		44 s	31 s	11
ZnO/α-Fe_2O_3 composites	290 °C	20 ppm	<8	3 s	36 s	35
Pt-decorated SnO_2 NWs	200 °C	500 ppm	8421	48 s	2 s	36
SnO_2 NW network	296 °C	100 ppm	326.4	0.42 s	108.8 s	37
La_2O_3-coated SnO_2 NWs	400 ∘C	100 ppm	57.3	1 s	110 s	38
$Zn_{1-x}Cd_xS$ (x = 0.4) NWs	206 °C	20 ppm	12.8	2 s	1 s	
		100 ppm	29	3 s	2 s	his work

recovery speeds are excellent candidates for high performance gas sensors. However, the work on sensing properties of composite $Zn_{1-x}Cd_xS$ has not been reported so far. The corresponding sensing mechanism is necessary to be discussed here for further research. It can be explained using a model, which mainly involves gas adsorption, charge transfer and desorption processes. As presented in Figure S3, I−V characteristics of the sensors in air show ohmic behavior. Therefore, the resistance of each sensor and the response are determined by the electroconductivity of the sensing film. When the $Zn_{1-x}Cd_xS$ NWs are surrounded by air, oxygen molecules are adsorbed on the NW surface to form oxygen ions (O_2^-, O^-, and O^{2-}) by capturing electrons from the conduction band of $Zn_{1-x}Cd_xS$ NWs, resulting in the formation of depletion regions at NWs surface and potential barriers at the NWs-NWs junctions. As shown in Scheme 1a, the existence of the depletion layers effectively generates a modified potential well that confines carriers into a region smaller than the geometrical size of the NW.[26] At the same time, the oxygen-adsorption-induced potential energy barrier at the intersection blocked the electron flow. As shown in the Scheme 1a, E_{CB} is the conduction band minimum, E_{VB} is the valence band maximum, and φ is the potential energy barrier at the intersection. Due to the formation of space-charge regions on the NW surface and the potential barriers at the NW−NW junctions, NW film shows a high resistance state in air. When the reductive ethanol gas is introduced, the charge transferring process begins. The ethanol molecule will contact with and then physically adsorbs onto the surface of NWs. The molecules of ethanol interact with adsorbed oxygen ions on the NWs surface and then release the trapped electrons back into the NWs, leading to thinner space-charge regions and lower potential barriers which decreased the resistance of the sensing NWs film. O^- is believed to be dominant at the operating temperature around 200 °C.[27] Therefore, the process of the reaction in our work can be described as follows:[28]

$$C_2H_5OH\ (gas) \leftrightarrow C_2H_5OH\ (ads) \quad (1)$$

$$C_2H_5OH\ (ads) + 6O^-\ (ads) \rightarrow 2CO_2 + 3H_2O + 6e^- \quad (2)$$

After that, when the sensors are exposed back to air, the electron capturing process starts, which increases the resistance of the sensing NWs film.

Compared with the pure ZnS NWs, $Zn_{1-x}Cd_xS$ show apparently enhanced responses with the increase of x value and obtained a max response value at x = 0.4. After that, the response decreased with the further increase of x value in the range of 0.6−1. This interesting phenomenon may be attributed to the dynamic equilibrium of two factors: the enhancement of the oxygen molecules absorption process and the increase of carrier intensity in the NWs. (1) Enhancement of the oxygen molecule absorption process is beneficial for the high response.

Scheme 1. Mechanisms Responsible for the Resistance Changes in NW-Based Gas Sensors[a]

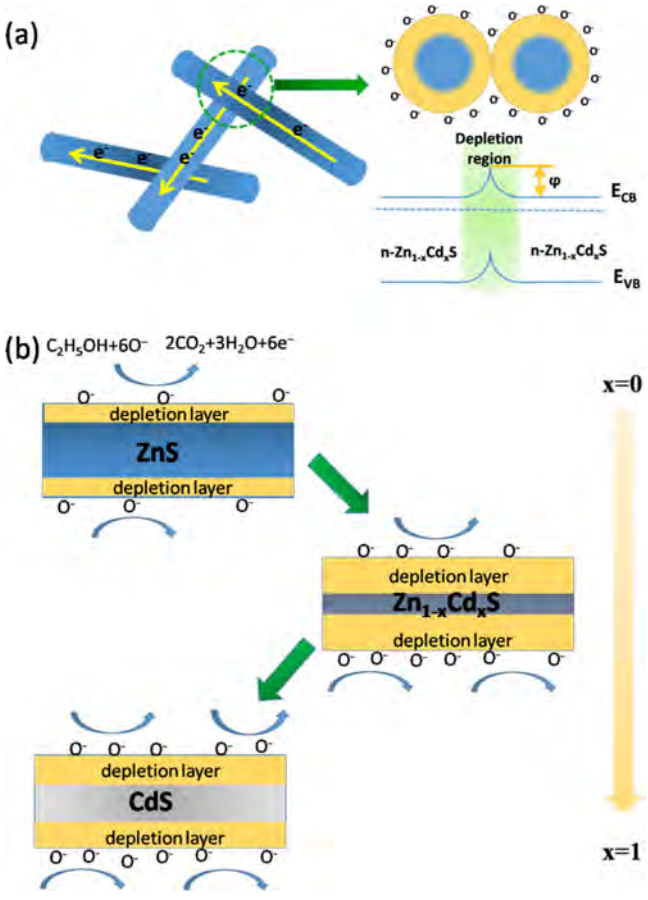

[a](a) Interfacial mechanisms for the crossed $Zn_{1-x}Cd_xS$ NWs. (b) Dynamic equilibrium of two factors: the enhancement of the oxygen molecules absorption process and the increase of carrier intensity in the NWs in $Zn_{1-x}Cd_xS$ NWs with the increase of x value.

DOI: 10.1021/acsami.5b05845
ACS Appl. Mater. Interfaces 2015, 7, 20793−20800

Once ZnS was incorporated with Cd, there were Cd−S chemical bonds appeared in the NWs. As reported by Lu et al., due to the smaller radius of Zn atom than Cd atom, Zn−S bond lengths are shorter than those of Cd−S bond. Zn−S bonds lengths of the $Cd_{1-x}Zn_xS$ (x = 0−1) solid are in the range of 2.36−2.40 Å while Cd−S bonds lengths in the rage of 2.52−2.58 Å.[39] It is generally known that when the ionic bond length is longer, the bond strength is weaker. Therefore, ionic bonds of Cd−S are weaker than those of Zn−S. Due to the weaker ionic bonds of Cd−S, it is easier for the adsorbed oxygen molecules to attract electrons from the conduction band of the $Zn_{1-x}Cd_xS$ once the Cd is incorporated. The active sites around Cd cations attracted more oxygen molecules and more oxygen ions are formed on the NWs surface. Therefore, the oxygen-adsorption-induced depletion layer width becomes larger and the barrier height at the NW−NW junctions gets higher, which benefit the increase of the sensing response. (2) The increase of carrier intensity in sensing material will lead to a thinner surface depletion layer. We can know that Cd acts as donor in the ZnS and the Cd incorporation increase the carrier intensity of the NWs. The surface depletion layer width is reported to be inversely proportional to the square root of electron concentration in n-type nanostructure.[26] With the increase of stoichiometric ratio of Cd:Zn, carrier intensity in the $Zn_{1-x}Cd_xS$ becomes larger and hence the surface depletion layer width will decrease, which goes against the obvious resistance change of the sensor before and after exposed to target gas. In our work, the two factors above may be used to explain the interesting sensing performances of the $Zn_{1-x}Cd_xS$ series sensors. When the x value is small, enhancement of the oxygen molecule absorption process may dominate the sensing mechanism. The more Cd is incorporated into the NWs, the more oxygen molecule ions are formed on the NW surface, and hence, the surface depletion layer becomes wider and the barrier height gets higher. In this way, the resistance of the NWs based device will change obviously when detecting ethanol gas. When x = 0.4, a maximum response value is obtained. However, when x becomes larger than 0.4, the increase of carrier intensity pays a more significant role in the regulation of the surface depletion layer width. Hence, the decrease of surface depletion layer width reduced the response to the target gas. The dynamic equilibrium sensing mechanism was shown in Scheme 1b.

The advantage of $Zn_{1-x}Cd_xS$ (x > 0) in a fast response performance might be attributed to the formation of Cd−S in NWs. The easier reaction process between oxygen molecules and the $Zn_{1-x}Cd_xS$ (x > 0) sensing film benefits the quick adsorption and desorption of the oxygen molecules, leading to the much quicker response and recovery speed of the $Zn_{1-x}Cd_xS$ (x > 0) than those of the binary ZnS.

The gas sensing selectivity is another important parameter to evaluate the sensing ability of semiconductor materials for practical applications, ensuring that the sensors can exactly detect the targeted molecules when they are exposed to the multi-component gas environment. Thus, the responses of the $Zn_{1-x}Cd_xS$ NW-based gas sensor to 100 ppm various gases, such as methanol (CH_3OH), ethanol (CH_3CH_2OH), acetone (C_3H_6O), formaldehyde (HCHO), benzene (C_6H_6), methyl-benzene (C_7H_8), xylene (C_8H_{10}), and so on were investigated at 206 °C. As shown in Figure 7, the six sensors exhibited much higher response to ethanol than other test gases, indicating that the $Zn_{1-x}Cd_xS$ NW is a good candidate for highly selective detection of ethanol. Among the six devices, the gas responses of the $Zn_{1-x}Cd_xS$ (x > 0) NWs sensor to ethanol were all larger than that of ZnS based sensor, and the largest response can be

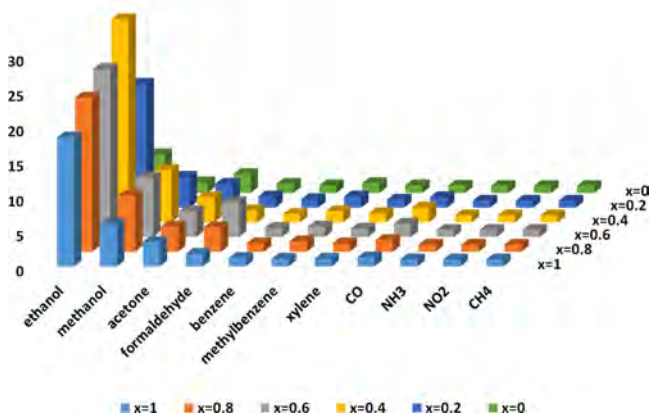

Figure 7. Sensing sensitivities of the gas sensors to different gases (100 ppm) at an operating temperature of 206 °C under a relative humidity of 25% RH.

observed for x = 0.4, which is more than 3-fold of the response to methanol gas with same concentration, indicating the better selectivity of the $Zn_{1-x}Cd_xS$ (x = 0.4) NWs sensor. It is worth mentioning that the sensors in this work also presented evident discrimination between ethanol and acetone which are similar materials. This may be due to the different LUMO energies of the two gases. In previous study, the selectivity of gas sensor to different volatile organic compound (VOC) molecules at different operating temperatures is considered to be due to the distinction of the orbital energies of the gases.[40] When the value of the LUMO energy is lower, the energy needed for the gas sensing reaction will reduce. As ethanol is reported to have lower LUMO energy value (0.12572 eV) than that of acetone (0.20525 eV), the ability of ethanol to capture electrons is stronger than that of acetone.[40] Therefore, the possibility of electron transfer between the ethanol molecules and surface of sensing NWs will be larger, leading to higher sensitivity of sensor to ethanol than acetone.

The ethanol sensing performance under different humid conditions is also demonstrated in Figure 8. From Figure 8a, it can be known that the sensors show different responses to 100 ppm ethanol gas under different humidity: when the humidity ranged from 15% to 50% RH, the responses increase with the humidity. Then, the sensor responses reached the highest when the relative humidity becomes 50% RH. After that, the figure clearly demonstrates a tendency of decrease in responses with humidity increasing from 50% to 90% RH. Therefore, it can be concluded that the humidity has a large effect on the response values of the sensors. It is reported by Bai et al. that the water adsorption should accelerate the oxygen adsorption to a certain extent on the sensing material surface and the total concentration of oxygen adsorption sites will increase with RH when the value of RH is low.[41] This may be the reason for the enhanced responses of the sensors with the increasing humidity from 15% to 50% RH in this work. However, when relative humidity increases further from 50% to 90% RH, the level of RH is too high, so that there are large amounts of water molecules adsorbed and many hydroxyl groups OH^- formed on the sensing material surface.[41] Due to the decrease of the effective surface area, less oxygen species are chemisorbed on the NWs surface, which goes against the sensitivity of the sensors. Therefore, the response decreases with RH increasing from 50% to 90% RH. Figure 8b and c shows the rise and recovery time of $Zn_{1-x}Cd_xS$ NWs sensors with x = 0, 0.4, and 1 under different humidity conditions

DOI: 10.1021/acsami.5b05845
ACS Appl. Mater. Interfaces 2015, 7, 20793−20800

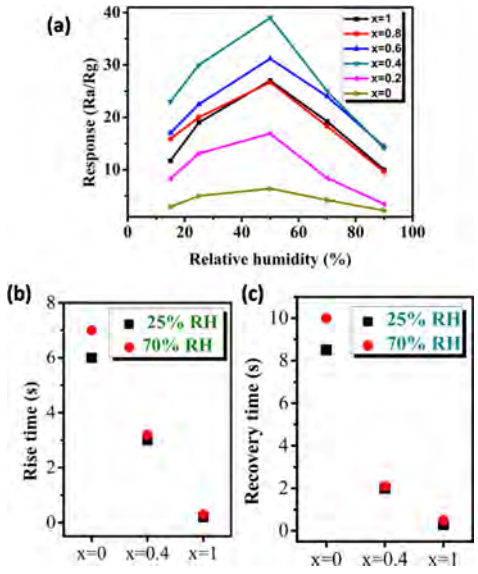

Figure 8. (a) Response values of sensors to 100 ppm ethanol gas under different humid conditions (15%, 25%, 50%, 70%, and 90% RH) at an operating temperature of 206 °C. (b) Rise and (c) recovery time of $Zn_{1-x}Cd_xS$ NWs sensors with $x = 0$, 0.4, and 1 to 100 ppm ethanol under different humidity conditions (25% and 70% RH).

(25% and 70% RH), demonstrating that the variation ranges of the rise and recovery time are small.

Stability is another prerequisite for reliable applications of chemical sensors. The stabilities of the sensors in 100 days (in Figure S4) have been examined, showing that the as-prepared sensors had response roughly comparable to the initial values for a long time while the response values fluctuated obviously. Further effort needs to be devoted to improve the sensor stability for practical applications.

CONCLUSIONS

Controlling the electrical and chemical properties of II−VI nanostructures is vital to their practical applications. In this work, $Zn_{1-x}Cd_xS$ NWs were synthesized by a one-step solvothermal method and used as novel materials for gas sensing application for the first time. Such $Zn_{1-x}Cd_xS$ NWs exhibit enhanced sensing performances compared with binary ZnS NWs. Especially, the sensor based on the $Zn_{1-x}Cd_xS$ (x = 0.4) NWs shows a large sensor response (s = 12.8), quick rise time (2 s), and quick recovery time (1 s) at 206 °C toward 20 ppm ethanol. A dynamic equilibrium mechanism of oxygen molecule absorption process and carrier intensity change in the NWs was used to explain the higher response of $Zn_{1-x}Cd_xS$. The easier reaction process between oxygen molecules and the $Zn_{1-x}Cd_xS$ ($x > 0$) sensing film is expected to be the reason for the much quicker response and recovery speed of the $Zn_{1-x}Cd_xS$ NWs than those of the binary ZnS NWs. The excellent sensing properties make these materials interesting not only for use in sensor devices, but also for a number of related electrochemical applications.

ASSOCIATED CONTENT

Supporting Information

The Supporting Information is available free of charge on the ACS Publications website at DOI: 10.1021/acsami.5b05845.

Process of preparing target gas with a certain concentration in a chamber. Schematic images of the ceramic tube coated with the sensing material and of the device and sensors with different x values. EDX data of $Zn_{1-x}Cd_xS$ NWs. Current−voltage characteristics of the sensors tested in air (25% RH) at room temperature. Stabilities of the sensors in 100 days examined at 206 °C (25% RH). Corresponding Zn, Cd and S atom % for $Zn_{1-x}Cd_xS$ NWs with different x values in precursor solution measured by EDS (PDF)

AUTHOR INFORMATION

Corresponding Authors

*E-mail: sp_wen@jlu.edu.cn.
*E-mail: chenyu@semi.ac.cn.
*E-mail: ruansp@jlu.edu.cn.

Author Contributions

The manuscript was written through contributions of all authors. All authors have given approval to the final version of the manuscript.

Notes

The authors declare no competing financial interest.

ACKNOWLEDGMENTS

This work was supported by National Natural Science Foundation of China (Grants 61274068, 61370046), the National High Technology Research and Development Program of China (Grant No. 2013AA030902), Opened Fund of the State Key Laboratory on Integrated Optoelectronics (No. IOSKL2013KF10), and Project of Science and Technology Plan of Changchun City (Grant No. 14KG020).

REFERENCES

(1) Zhai, T.; Fang, X.; Li, L.; Bando, Y.; Golberg, D. One-dimensional CdS Nanostructures: Synthesis, Properties, and Applications. *Nanoscale* **2010**, *2*, 168−187.
(2) Park, S.; An, S.; Ko, H.; Lee, S.; Lee, C. Synthesis, Structure, and UV-enhanced Gas Sensing Properties of Au-functionalized ZnS Nanowires. *Sens. Actuators, B* **2013**, *188*, 1270−1276.
(3) Moore, D.; Wang, Z. L. Growth of Anisotropic One-dimensional ZnS Nanostructures. *J. Mater. Chem.* **2006**, *16*, 3898−3905.
(4) Goudarzi, A.; Aval, G. M.; Sahraei, R.; Ahmadpoor, H. Ammonia-free Chemical Bath Deposition of Nanocrystalline ZnS Thin Film Buffer Layer for Solar Cells. *Thin Solid Films* **2008**, *516*, 4953−4957.
(5) Chen, Z.-G.; Cheng, L.; Xu, H.-Y.; Liu, J.-Z.; Zou, J.; Sekiguchi, T.; Lu, G. Q.; Cheng, H.-M. ZnS Branched Architectures as Optoelectronic Devices and Field Emitters. *Adv. Mater.* **2010**, *22*, 2376−2380.
(6) He, J. H.; Zhang, Y. Y.; Liu, J.; Moore, D.; Bao, G.; Wang, Z. L. ZnS/Silica Nanocable Field Effect Transistors as Biological and Chemical Nanosensors. *J. Phys. Chem. C* **2007**, *111*, 12152−12156.
(7) He, Y.; Wang, H.-F.; Yan, X.-P. Exploring Mn-doped ZnS Quantum Dots for the Room-Temperature Phosphorescence Detection of Enoxacin in Biological Fluids. *Anal. Chem.* **2008**, *80*, 3832−3837.
(8) Jiang, P.; Jie, J.; Yu, Y.; Wang, Z.; Xie, C.; Zhang, X.; Wu, C.; Wang, L.; Zhu, Z.; Luo, L. Aluminium-doped N-type ZnS Nanowires as High-performance UV and Humidity Sensors. *J. Mater. Chem.* **2012**, *22*, 6856−6861.
(9) Ahn, M. W.; Park, K. S.; Heo, J. H.; Park, J. G.; Kim, D. W.; Choi, K. J.; Lee, J. H.; Hong, S. H. Gas Sensing Properties of Defect-controlled ZnO-nanowire Gas Sensor. *Appl. Phys. Lett.* **2008**, *93*, 263103.
(10) Liu, Y.; Jiao, Y.; Zhang, Z.; Qu, F.; Umar, A.; Wu, X. Hierarchical SnO_2 Nanostructures Made of Intermingled Ultrathin Nanosheets for Environmental Remediation, Smart Gas Sensor, and Supercapacitor Applications. *ACS Appl. Mater. Interfaces* **2014**, *6*, 2174−2184.
(11) Zhu, L.; Zhang, D.; Wang, Y.; Feng, C.; Zhou, J.; Liu, C.; Ruan, S. Xylene Gas Sensor Based On Ni Doped TiO_2 Bowl-like Submicron Particles With Enhanced Sensing Performance. *RSC Adv.* **2015**, *5*, 28105−28110.

DOI: 10.1021/acsami.5b05845
ACS Appl. Mater. Interfaces 2015, 7, 20793−20800

(12) Chen, Y.; Zhu, L.; Feng, C.; Liu, J.; Li, C.; Wen, S.; Ruan, S. Low Temperature Operating $In_{2-x}Ni_xO_3$ Sensors With High Response and Good Selectivity for NO_2 Gas. *J. Alloys Compd.* **2013**, *581*, 653−658.
(13) Zhang, Z.; Li, X.; Wang, C.; Wei, L.; Liu, Y.; Shao, C. ZnO Hollow Nanofibers: Fabrication From Facile Single Capillary Electrospinning and Applications in Gas Sensors. *J. Phys. Chem. C* **2009**, *113*, 19397−19403.
(14) Eranna, G.; Joshi, B. C.; Runthala, D. P.; Gupta, R. P. Oxide Materials for Development of Integrated Gas Sensors—a Comprehensive Review. *Crit. Rev. Solid State Mater. Sci.* **2004**, *29*, 111−188.
(15) Carotta, M. C.; Cervi, A.; di Natale, V.; Gherardi, S.; Giberti, A.; Guidi, V.; Puzzovio, D.; Vendemiati, B.; Martinelli, G.; Sacerdoti, M.; Calestani, D.; Zappettini, A.; Zha, M.; Zanotti, L. ZnO Gas Sensors: a Comparison Between Nanoparticles and Nanotetrapods-based Thick Films. *Sens. Actuators, B* **2009**, *137*, 164−169.
(16) Wei, A.; Pan, L.; Huang, W. Recent Progress in the ZnO Nanostructure-based Sensors. *Mater. Sci. Eng., B* **2011**, *176*, 1409−1421.
(17) Wang, X.; Xie, Z.; Huang, H.; Liu, Z.; Chen, D.; Shen, G. Gas Sensors, Thermistor and Photodetector Based on ZnS Nanowires. *J. Mater. Chem.* **2012**, *22*, 6845−6850.
(18) Siemons, M.; Leifert, A.; Simon, U. Preparation and Gas Sensing Characteristics of Nanoparticulate P-Type Semiconducting $LnFeO_3$ and $LnCrO_3$ Materials. *Adv. Funct. Mater.* **2007**, *17*, 2189−2197.
(19) Cao, M.; Wang, Y.; Chen, T.; Antonietti, M.; Niederberger, M. A Highly Sensitive and Fast-responding Ethanol Sensor Based on $CdIn_2O_4$ Nanocrystals Synthesized by A Nonaqueous Sol−gel Route. *Chem. Mater.* **2008**, *20*, 5781−5786.
(20) Zhu, L.; Feng, C.; Li, F.; Zhang, D.; Li, C.; Wang, Y.; Lin, Y.; Ruan, S.; Chen, Z. Excellent Gas Sensing and Optical Properties of Single-crystalline Cadmium Sulfide Nanowires. *RSC Adv.* **2014**, *4*, 61691−61697.
(21) Kim, D. S.; Cho, Y. J.; Park, J.; Yoon, J.; Jo, Y.; Jung, M.-H. Mn, Zn) Co-Doped CdS Nanowires. *J. Phys. Chem. C* **2007**, *111*, 10861−10868.
(22) Biswas, S.; Kar, S.; Santra, S.; Jompol, Y.; Arif, M.; Khondaker, S. I. Solvothermal Synthesis of High-aspect Ratio Alloy Semiconductor Nanowires: $Cd_{1-x}Zn_xS$, a Case Study. *J. Phys. Chem. C* **2009**, *113*, 3617−3624.
(23) Dong, L.; Liu, Y.; Zhuo, Y.; Chu, Y. General Route to the Fabrication of ZnS and M-Doped (M = Cd^{2+}, Mn^{2+}, Co^{2+}, Ni^{2+}, and Eu^{3+}) ZnS Nanoclews and a Study of Their Properties. *Eur. J. Inorg. Chem.* **2010**, *2010*, 2504−2513.
(24) Jiang, Y.; Meng, X. M.; Liu, J.; Xie, Z. Y.; Lee, C. S.; Lee, S. T. Hydrogen-assisted Thermal Evaporation Synthesis of ZnS Nanoribbons on a Large Scale. *Adv. Mater.* **2003**, *15*, 323−327.
(25) Pan, A. L.; Wang, S. Q.; Liu, R. B.; Li, C. R.; Zou, B. S. Thermal Stability and Lasing of US Nanowires Coated by Amorphous Silica. *Small* **2005**, *1*, 1058−1062.
(26) Li, D.; Zhang, J.; Xiong, Q. 30 nm Surface Depletion Induced Quantum Confinement in CdS Nanobelts. *ACS Nano* **2012**, *6*, 5283−5290.
(27) Barsan, N.; Schweizer-Berberich, M.; Göpel, W. Fundamental and Practical Aspects in the Design of Nanoscaled SnO_2 Gas Sensors: a Status Report. *Fresenius' J. Anal. Chem.* **1999**, *365*, 287−304.
(28) Xue, X.; Chen, Z.; Ma, C.; Xing, L.; Chen, Y.; Wang, Y.; Wang, T. One-step Synthesis and Gas-sensing Characteristics of Uniformly Loaded Pt@SnO_2 Nanorods. *J. Phys. Chem. C* **2010**, *114*, 3968−3972.
(29) Men, H.; Gao, P.; Zhou, B.; Chen, Y.; Zhu, C.; Xiao, G.; Wang, L.; Zhang, M. Fast Synthesis of Ultra-thin $ZnSnO_3$ Nanorods With High Ethanol Sensing Properties. *Chem. Commun.* **2010**, *46*, 7581−7583.
(30) Huang, J.; Yu, K.; Gu, C.; Zhai, M.; Wu, Y.; Yang, M.; Liu, J. Preparation of Porous Flower-shaped SnO_2 Nanostructures and Their Gas-sensing Property. *Sens. Actuators, B* **2010**, *147*, 467−474.
(31) Liu, X.; Zhang, J.; Wang, L.; Yang, T.; Guo, X.; Wu, S.; Wang, S. 3D Hierarchically Porous ZnO Structures and Their Functionalization by Au nanoparticles for Gas Sensors. *J. Mater. Chem.* **2011**, *21*, 349−356.
(32) Kamble, A. S.; Pawar, R. C.; Tarwal, N. L.; More, L. D.; Patil, P. S. Ethanol Sensing Properties of Chemosynthesized CdO Nanowires and Nanowalls. *Mater. Lett.* **2011**, *65*, 1488−1491.
(33) Xiangfeng, C.; Dongli, J.; Yu, G.; Chenmou, Z. Ethanol Gas Sensor Based on $CoFe_2O_4$ Nano-crystallines Prepared by Hydrothermal Method. *Sens. Actuators, B* **2006**, *120*, 177−181.
(34) Li, L.; Liu, M.; He, S.; Chen, W. Freestanding 3D Mesoporous Co_3O_4@carbon Foam Nanostructures for Ethanol Gas Sensing. *Anal. Chem.* **2014**, *86*, 7996−8002.
(35) Zhou, X.; Xiao, Y.; Wang, M.; Sun, P.; Liu, F.; Liang, X.; Li, X.; Lu, G. Highly Enhanced Sensing Properties for ZnO Nanoparticle-decorated Round-edged α-Fe_2O_3 Hexahedrons. *ACS Appl. Mater. Interfaces* **2015**, *7*, 8743−8749.
(36) Lin, Y.; Hsueh, Y.; Lee, P.; Wang, C.; Wu, J.; Perng, T.; Shih, H. C. Fabrication of Tin Dioxide Nanowires with Ultrahigh Gas Sensitivity by Atomic Layer Deposition of Platinum. *J. Mater. Chem.* **2011**, *21*, 10552.
(37) Hwang, I.; Kim, S.; Choi, J.; Jung, J.; Yoo, D.; Dong, K.; Ju, B.; Lee, J. Large-scale Fabrication of Highly Sensitive SnO_2 Nanowire Network Gas Sensors by Single Step Vapor Phase Growth. *Sens. Actuators, B* **2012**, *165*, 97−103.
(38) Van Hieu, N.; Kim, H.; Ju, B.; Lee, J. Enhanced Performance of SnO_2 Nanowires Ethanol Sensor by Functionalizing with La_2O_3. *Sens. Actuators, B* **2008**, *133*, 228−234.
(39) Lu, J.; Dai, Y.; Guo, M.; Wei, W.; Ma, Y.; Han, S.; Huang, B. Structure and Electronic Properties and Phase Stabilities of the $Cd_{1-x}Zn_xS$ Solid Solution in the Range of 0-x-1. *ChemPhysChem* **2012**, *13*, 147−154.
(40) Wen, Z.; Tian-mo, L. Gas-sensing Properties of SnO_2-TiO_2-based Sensor for Volatile Organic Compound Gas and Its Sensing Mechanism. *Phys. B* **2010**, *405*, 1345−1348.
(41) Bai, Z.; Xie, C.; Hu, M.; Zhang, S.; Zeng, D. Effect of Humidity on the Gas Sensing Property of the Tetrapod-shaped ZnO Nanopowder Sensor. *Mater. Sci. Eng., B* **2008**, *149*, 12−17.

DOI: 10.1021/acsami.5b05845
ACS Appl. Mater. Interfaces 2015, 7, 20793−20800